Polarization-Dependent Interference of Coherent Scattering from Orthogonal Dipole Moments of a Resonantly Excited Quantum Dot

Disheng Chen,[1] Gary R. Lander,[1] Glenn S. Solomon,[2] and Edward B. Flagg[1,*]
[1]Department of Physics and Astronomy, West Virginia University, Morgantown, West Virginia 26506, USA
[2]Joint Quantum Institute, National Institute of Standards and Technology, and University of Maryland, Gaithersburg, Maryland 20889, USA

(Received 29 August 2016; revised manuscript received 15 November 2016; published 20 January 2017)

Resonant photoluminescence excitation (RPLE) spectra of a neutral InGaAs quantum dot show unconventional line shapes that depend on the detection polarization. We characterize this phenomenon by performing polarization-dependent RPLE measurements and simulating the measured spectra with a three-level quantum model. The spectra are explained by interference between fields coherently scattered from the two fine structure split exciton states, and the measurements enable extraction of the steady-state coherence between the two exciton states.

DOI: 10.1103/PhysRevLett.118.037401

Light-matter interactions in semiconductor nanostructures have attracted significant research interest because of both fundamental physics questions and practical concerns. Epitaxially grown quantum dots (QDs), with their narrow emission linewidths and atomlike density of states in a solid-state system, are archetypical elements of study and are potentially useful for many reasons. For example, they have been demonstrated to be efficient sources for single photons [1,2] and entangled photon pairs [3,4], both of which are capabilities applicable to quantum information science. Resonant continuous wave (cw) excitation of the bound exciton states has allowed measurement of a number of phenomena that cannot be seen with either incoherent or pulsed excitation. Some examples are the Mollow triplet emission from dressed states of a two-level quantum system [5–7] and the related Mollow quintuplet from dressed states of a V system [8]. The selectivity and precision of resonant excitation have also allowed the production of high-indistinguishability photons [9,10] and measurement of charge and spin fluctuations in the local solid-state environment [11–13]. Many resonant excitation experiments use crossed polarizers to attenuate the laser scattering and allow detection of the resonance fluorescence [10–12,14–16]. In such a case, the fluorescence detection is necessarily polarization selective. Here we show that when polarization-selective detection is used, orthogonal dipole moments, such as those of a neutral QD or those of a charged QD in a transverse magnetic field, cause an interference effect that results in an unconventionally shaped excitation spectrum.

In typical epitaxially grown quantum dots, the anisotropic exchange interaction results in two bound exciton states split by several μeV with orthogonal transition dipole moments that emit linearly polarized fluorescence [17–20]. When the fine structure splitting is on the order of the transition linewidth, a cw excitation laser can interact with both exciton states simultaneously if it is polarized so as to have a nonzero projection onto both dipole moments. The QD-field interaction will cause both coherent scattering at the laser frequency [5,21,22] and incoherent spontaneous emission at the transition dipole frequencies. The fields coherently scattered from the two nondegenerate orthogonal dipoles will be at the same frequency but phase shifted relative to each other. Interference between these fields results in a noticeable difference between the shapes of the excitation spectra for detection polarizations parallel and orthogonal to the excitation. This phenomenon is not present in pulsed excitation experiments, where the emission is generally unpolarized when both dipole moments are excited [23]. By measuring polarization-dependent excitation spectra for polarizations both aligned to the transition dipole moments and 45-deg rotated relative to them, we can extract the real part of the coherence between the two fine structure states induced by the excitation.

The sample studied in this work consists of self-assembled InGaAs QDs embedded in a 4-λ GaAs waveguide bounded by two AlGaAs/GaAs distributed Bragg reflectors, which form a planar microcavity. The sample is maintained at 4.2 K in a closed-cycle cryostat. The energy level structure of a neutral QD is depicted in Fig. 1(a), and the associated dipole moment orientations are shown in Fig. 1(b). The system is investigated using polarization-dependent resonant photoluminescence excitation (RPLE) spectroscopy, which measures the total fluorescence from the QD as the frequency of the cw excitation laser is scanned across the QD resonance. Multiple RPLE spectra are recorded using different detection polarizations under the same excitation polarization. Rather than using crossed polarizers to discriminate between fluorescence and laser scattering [14,15], we instead use modal discrimination between the waveguide mode and the Fabry-Perot mode of the planar microcavity [6–8,13]. A resonant laser with a 1 MHz linewidth is coupled into the waveguide mode through the cleaved edge of the sample.

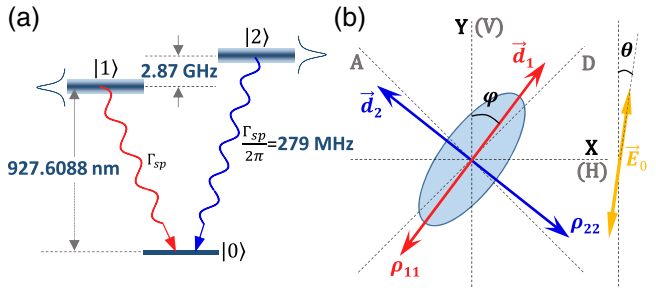

FIG. 1. (a) Quantum dot energy diagram. The population spontaneous decay rate is determined to be $\Gamma_{sp}/2\pi = (279.2 \pm 0.9)$ MHz by time-resolved fluorescence measurements (see Supplemental Material [24]), and the fine structure splitting is $\Delta_{FSS}/2\pi = (2.869 \pm 0.001)$ GHz. (b) Polarization and electric dipole moment orientations. The lower-energy $\boldsymbol{d}_1$ and higher-energy $\boldsymbol{d}_2$ dipole moments are shown, as is the polarization of the excitation field $\boldsymbol{E}_0$. The shape of the QD is shown schematically with its asymmetry exaggerated.

The photoluminescence (PL) is coupled out through the Fabry-Perot mode normal to the sample plane. It is first collimated by an aspheric objective lens with N.A. = 0.5, and then guided through a pair of liquid crystal variable retarders (LCVRs) and a linear polarizer. The light then enters a monochromator to select the PL from just one QD, which is detected by a thermoelectrically cooled CCD camera and spectrally integrated. The fast axes of the two LCVRs are aligned to the vertical and diagonal directions, allowing us to rotate any polarization state onto the measurement axis determined by the linear polarizer. Therefore, we can fully characterize the polarization state of the PL via the Stokes vector by measuring the intensity projection on the horizontal (X), vertical (Y), diagonal (D), antidiagonal (A), left-circular (L), and right-circular (R) polarizations.

Figures 2(a) and 2(b) show two normalized RPLE spectra under the same excitation conditions but with different detection polarizations: horizontal (X) or vertical (Y). Neither spectrum can be reconstructed by incoherently adding two Lorentzian lines centered at the two peaks, as would be the case if the fluorescence consisted solely of spontaneous emission. This implies that to account for the observed unconventional line shapes, we must also include a polarization-dependent interference occurring between photons coherently scattered by the two fine structure states. Clear evidence of the presence of such interference can be seen at zero detuning, where a 90° polarization switching with respect to the excitation field is present; i.e., the scattered light becomes highly X polarized even though the excitation is Y polarized.

An analysis of the proportions of coherent and incoherent scattering in these spectra illustrates the underlying physics. In Figs. 2(a) and 2(b), these calculated proportions are denoted by the green (solid) and red (dashed) lines for coherent and incoherent scattering, respectively. As expected, the incoherent scattering looks much like the incoherent sum of two Lorentzians; the small overlap of the two peaks leads to a negligible contribution at zero detuning. In contrast, because the coherent scattering is always at the laser wavelength, a pronounced interference effect is expected between contributions from the two dipoles. The relative phase shift of the coherently scattered photons is determined by the detuning of the laser with

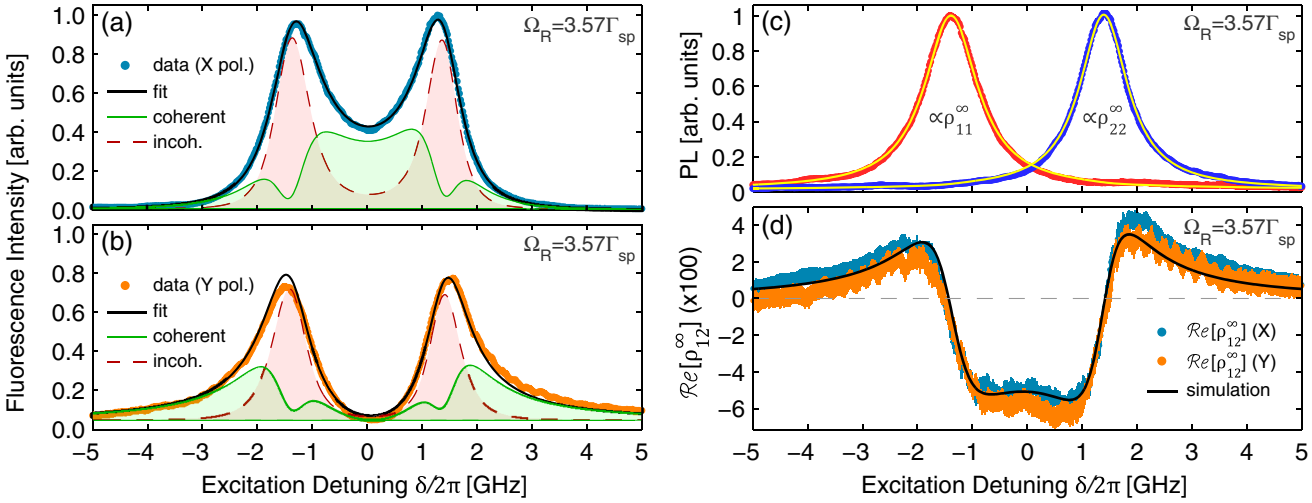

FIG. 2. Example RPLE spectra recorded with $\Omega_R = 3.57\Gamma_{sp}$ and detection polarization chosen to be (a) X (blue points), (b) Y (orange points), or (c) to eliminate either the low-energy or high-energy peak. The black solid lines in (a) and (b) are fittings following Eqs. (1) and (2). The green (solid) and red (dashed) lines underneath the spectra are the calculated portions of coherent and incoherent scattering, respectively. The two yellow curves in (c) are the fittings obtained by using the calculated exciton populations ρ^{∞}_{11} and ρ^{∞}_{22} from the three-level model. (d) The coherence $\mathrm{Re}[\rho^{\infty}_{12}]$ extracted from the curves in (a) and (b); the colors indicate the polarization whence the coherence was extracted. The black solid curve in (d) is not a fit but the calculation of $\mathrm{Re}[\rho^{\infty}_{12}]$ using the same parameters found in the previous fittings in (a) and (b).

respect to each transition energy. This is similar to a driven harmonic oscillator: red-detuned driving results in a negative (lagging) phase while blue-detuned driving leads to a positive (leading) phase. Thus at zero detuning, the fields coherently scattered from the two dipoles have a relative phase shift even though the field polarizations are still aligned to each dipole. The detection polarization determines whether these phase-shifted fields combine constructively [for horizontal (X) polarization] or destructively [for vertical (Y) polarization]. This explains the observed enhancement or diminution of the PL signal around zero detuning in Figs. 2(a) and 2(b), respectively.

In contrast to the excitation spectrum presented in Figs. 2(a) and 2(b), the emission spectrum for a resonantly excited neutral QD should be a Mollow quintuplet [8]. In the emission spectrum, the coherent scattering would appear as a delta function at the laser frequency, while the incoherent scattering from the dressed states [5,27] appears at the laser frequency and at four peaks beside it. Here the spectrometer resolution was not high enough to resolve the separate peaks, so the fluorescence was spectrally integrated and the excitation spectrum analyzed. In future work, the coherent portion of the fluorescence could be measured separately from the incoherent part via heterodyne measurements [22] and compared to the theoretical models in Figs. 2(a) and 2(b).

We model the neutral QD as a three-level V system and calculate its density matrix using a quantum master equation in Lindblad form [28,29]; we treat the excitation interaction semiclassically under the rotating wave approximation [28,30]. The scattered field, both coherent and incoherent parts, can be linked to elements of the density matrix [28,31]. The final expressions for the X- and Y-polarized and total RPLE intensities are as follows (see Supplemental Material [24] for the detailed derivation):

$$I_X = I_0\{\sin^2(\varphi)\rho_{11}^{\infty} + \cos^2(\varphi)\rho_{22}^{\infty} - \sin(2\varphi)\mathrm{Re}[\rho_{12}^{\infty}]\}, \tag{1}$$

$$I_Y = I_0\{\cos^2(\varphi)\rho_{11}^{\infty} + \sin^2(\varphi)\rho_{22}^{\infty} + \sin(2\varphi)\mathrm{Re}[\rho_{12}^{\infty}]\}, \tag{2}$$

$$I = I_X + I_Y = I_0\{\rho_{11}^{\infty} + \rho_{22}^{\infty}\}, \tag{3}$$

where ρ_{11}^{∞} and ρ_{22}^{∞} are the populations in levels $|1\rangle$ and $|2\rangle$, ρ_{12}^{∞} is the coherence between the two excited states, the superscript ∞ represents the steady-state solutions, and φ is the angle of the dipole moment $\boldsymbol{d_1}$ with respect to the Y axis [see Fig. 1(b)]. I_0 is the intensity constant, $I_0 = \omega_0^4 d^2/128\pi^4\epsilon_0 c^3 r^2$, where $d \approx |\boldsymbol{d}_1| \approx |\boldsymbol{d}_2|$ is the magnitude of the transition dipole moment, $\omega_0 = (\omega_1 + \omega_2)/2$ is the average transition frequency, and r is the distance from the QD to the detector. In this work, we label all the resonant excitation powers with the corresponding overall Rabi frequency $\Omega_R = d|\boldsymbol{E}_0|/\hbar$ in units of the population decay rate Γ_{sp}. The individual Rabi frequency Ω_j for level $|j\rangle$ is $\Omega_R \cos(\beta_j)$, where β_j is the angle between the electric dipole moment $\boldsymbol{d}_j$ and the excitation field $\boldsymbol{E}_0$.

The RPLE intensities in Eqs. (1) and (2) are not just proportional to the excited state populations ρ_{11}^{∞} and ρ_{22}^{∞}, which would be the case for a two-level system. Instead, they are modified by the real part of the coherence between the two excited states, i.e., $\mathrm{Re}[\rho_{12}^{\infty}]$. In contrast, the total PL intensity in Eq. (3) is still proportional to the total population in both excited states. The difference in the sign of the third terms in I_X and I_Y explains the difference between the X-polarized and Y-polarized RPLE spectra. By simultaneously fitting Eqs. (1) and (2) to multiple sets of RPLE spectra measured at different excitation powers, we determine the orientation of the dipole moment $\boldsymbol{d}_1$ to be $\varphi = 44.74° \pm 0.04°$ with respect to the Y axis, and the direction of the resonant excitation field $\boldsymbol{E}_0$ to be $\theta = 3.37° \pm 0.07°$ with respect to the Y axis. Thus, the electric dipole moments of the QD, $\boldsymbol{d}_1$ and $\boldsymbol{d}_2$, are almost aligned to the diagonal (D) and the antidiagonal (A) directions, respectively, which is consistent with our Stokes parameter measurement and analysis of the PL (see Supplemental Material [24]). $\boldsymbol{E_0}$ is nominally aligned to the Y axis because the excitation laser is propagating in the X direction along the waveguide mode. But $\boldsymbol{E_0}$ may deviate from that alignment due to unintentional non-normal incidence of the laser on the air-GaAs interface, which would cause refraction of the beam away from the X direction.

Figure 2(c) shows the RPLE spectra measured with the LCVRs tuned to block the PL emitted from either the high-energy or low-energy state of the fine structure doublet. Since that approach measures the emission from only one energy level at a time, there is no interference effect in these spectra. Each spectrum can be directly fitted with the corresponding excited population as $I_1 = A_1\rho_{11}^{\infty} + B_1$ and $I_2 = A_2\rho_{22}^{\infty} + B_2$ for states $|1\rangle$ and $|2\rangle$, respectively, where A_j and B_j are fitting parameters. To account for the polarization-dependent absorption of the optics in the detection path, we use the fact that both the sum of the spectra in Fig. 2(c) and the sum of the spectra in Figs. 2(a) and 2(b) are proportional to the total excited population in the QD (See Supplemental Material [24]). This ensures accurate extraction of the real part of the coherence $\mathrm{Re}[\rho_{12}^{\infty}]$, as shown in Fig. 2(d). Using parameters from the fits in Figs. 2(a) and 2(b), the three-level V-system simulation reproduces the shape of the coherence successfully [black curve in Fig. 2(d)].

Figure 3 shows the extracted real part of the coherence for multiple excitation powers. As the excitation power increases, the dispersive line shapes centered at each fine structure resonance increase in magnitude and experience power broadening, as is expected for coherent excitation [30]. Again, the simulations match the data well and even reproduce the slight asymmetry about zero detuning. We note that to obtain an observable asymmetry requires two conditions: (1) the dipole moments of the QD must not be

oriented 45 deg with respect to the excitation field, and (2) the excitation power must be high. The single condition of tilted QD dipole moments is not enough to achieve this asymmetry according to the simulations (see Supplemental Material [24]), implying that this is a nonlinear effect happening at high excitation power. In the inset of Fig. 3, the Rabi frequencies extracted from the fittings follow a linear relationship with respect to the square root of power, as expected.

There are several differences between the cw excitation used in this study and experiments that use pulsed excitation to create and measure coherence (see, e.g., Ref. [23]). Under pulsed excitation, a coherent superposition of two excited states is created by the excitation pulse, which then evolves freely over time and experiences quantum beats at a frequency determined by the fine structure splitting Δ_{FSS}. Since $\Delta_{\mathrm{FSS}} \gg \Gamma_{\mathrm{sp}}$, it most often leads to a vanishingly small polarization in the time-integrated fluorescence. In addition, the fluorescence is entirely spontaneous emission, which is incoherent; there is no coherent scattering. In contrast, under cw excitation, coherent scattering occurs and a strong polarization results. Moreover, the density matrix under cw excitation is in a steady state that depends on the excitation power and detuning, rather than a time-varying state.

The solid dots in Figs. 4(a) and 4(b) are the peak positions of the spectra in Fig. 2(c) obtained by fitting them each with a Lorentzian function (Fig. S3 in Supplemental Material [24]). We find that the two resonance peaks move towards each other as the power increases; this is due to the ac Stark effect. For example, when the laser is near resonance with the low-energy state $|1\rangle$, the excitation field is red detuned with respect to the high-energy state $|2\rangle$. This detuning pushes state $|0\rangle$ and state $|2\rangle$ away from each other via the ac Stark effect [32–34]. The redshift of the ground state in turn effectively increases the transition energy of state $|1\rangle$. Since the ac Stark effect gets stronger at higher excitation power, the low-energy state $|1\rangle$ moves continuously towards the higher-energy side of the spectrum. Similarly, the high-energy state $|2\rangle$ experiences a redshift in its transition energy as the power increases. We calculate the expected resonance positions based on the fitting parameters found in Fig. 2(a) and depict them as solid lines in Figs. 4(a) and 4(b). They are in good agreement with the data, especially for the high-energy state.

The open circles in Figs. 4(a) and 4(b) represent the fitting parameters $\omega_2/2\pi$ and $\omega_1/2\pi$, called the intrinsic

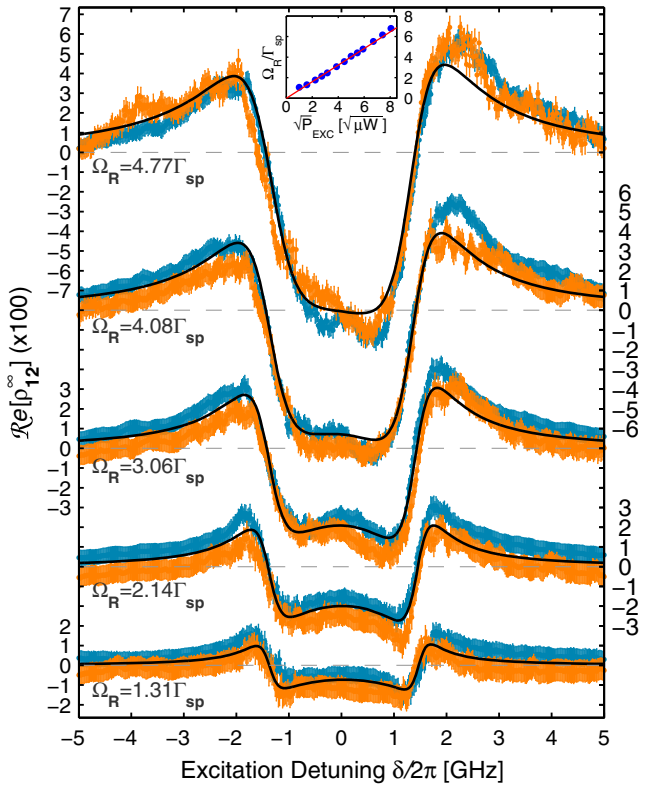

FIG. 3. $\mathrm{Re}[\rho^{\infty}_{12}]$ extracted at different excitation powers. The curves are vertically offset for clarity. The color scheme used in each pair is the same as Fig. 2(d); i.e., orange is extracted from the Y-polarized RPLE and blue from the X-polarized RPLE. The black solid curves are the calculation of $\mathrm{Re}[\rho^{\infty}_{12}]$ at different Rabi frequencies Ω_R determined by fittings to the raw RPLE data similar to Figs. 2(a) and 2(b). The other model parameters are the same throughout all the calculations. Inset: Rabi frequency Ω_R versus the square root of the excitation power. The red straight line is a linear fit with a slope of $(0.806 \pm 0.011)\Gamma_{\mathrm{sp}}/\sqrt{\mu W}$.

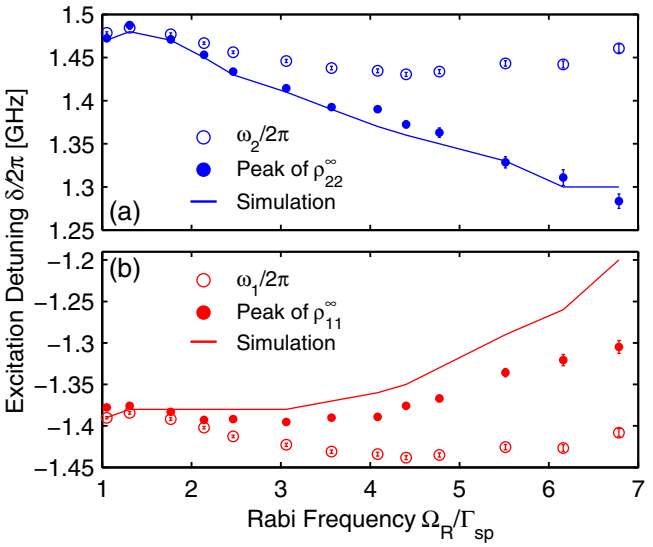

FIG. 4. (a) The evolution of the high-energy state's intrinsic resonance frequency $\omega_2/2\pi$ (blue open circles) and the evolution of the peak positions of the excited population ρ^{∞}_{22} obtained by either a Lorentzian fitting (blue dots) or the V-system simulation (blue line). (b) The evolution of the low-energy state's intrinsic resonance frequency $\omega_1/2\pi$ (red open circles) and the evolution of the peak positions of the excited population ρ^{∞}_{11} obtained by either a Lorentzian fitting (red dots) or the V-system simulation (red line).

transition frequencies for states $|2\rangle$ and $|1\rangle$. These parameters are determined by the intrinsic properties of the QD, which should not change if the QD's local environment is not disturbed. Therefore, the variation of $\omega_2/2\pi$ and $\omega_1/2\pi$ shown in Figs. 4(a) and 4(b) reflects the fluctuations of the local environment caused by the resonant excitation laser [13]. Further discussion on these fluctuations is given in Sec. 6 of the Supplemental Material [24].

In this Letter, we have demonstrated and modeled an interference effect that occurs during cw resonant excitation of a multilevel quantum system. Including coherent scattering is necessary to explain the strong polarization difference between the excitation and the emission. Such a phenomenon does not occur under incoherent or pulsed excitation. Comparison of spectra with different detection polarizations allows extraction of the steady-state coherence generated between the two excited states. All the spectra and coherences are correctly reproduced by a density matrix model of the QD. Similar effects must be accounted for in any situation where there are two nondegenerate orthogonal transition dipole moments and only a certain polarization is detected. One example is the "dark-field" resonant excitation and detection technique [15] in combination with a charged QD in an in-plane magnetic field.

We would like to acknowledge Tim Thomay for helpful discussions. This work was supported by the National Science Foundation (DMR-1452840).

*edward.flagg@mail.wvu.edu

[1] P. Michler, A. Kiraz, C. Becher, W. V. Schoenfeld, P. M. Petroff, L. Zhang, E. Hu, and A. Imamoglu, A quantum dot single-photon turnstile device, Science **290**, 2282 (2000).

[2] C. Santori, M. Pelton, G. Solomon, Y. Dale, and Y. Yamamoto, Triggered Single Photons from a Quantum Dot, Phys. Rev. Lett. **86**, 1502 (2001).

[3] N. Akopian, N. H. Lindner, E. Poem, Y. Berlatzky, J. Avron, D. Gershoni, B. D. Gerardot, and P. M. Petroff, Entangled Photon Pairs from Semiconductor Quantum Dots, Phys. Rev. Lett. **96**, 130501 (2006).

[4] R. Trotta, J. S. Wildmann, E. Zallo, O. G. Schmidt, and A. Rastelli, Highly entangled photons from hybrid piezoelectric-semiconductor quantum dot devices, Nano Lett. **14**, 3439 (2014).

[5] B. R. Mollow, Power spectrum of light scattered by two-level systems, Phys. Rev. **188**, 1969 (1969).

[6] A. Muller, E. B. Flagg, P. Bianucci, X. Y. Wang, D. G. Deppe, W. Ma, J. Zhang, G. J. Salamo, M. Xiao, and C. K. Shih, Resonance Fluorescence from a Coherently Driven Semiconductor Quantum Dot in a Cavity, Phys. Rev. Lett. **99**, 187402 (2007).

[7] E. B. Flagg, A. Muller, J. W. Robertson, S. Founta, D. G. Deppe, M. Xiao, W. Ma, G. J. Salamo, and C. K. Shih, Resonantly driven coherent oscillations in a solid-state quantum emitter, Nat. Phys. **5**, 203 (2009).

[8] R.-C. Ge, S. Weiler, A. Ulhaq, S. M. Ulrich, M. Jetter, P. Michler, and S. Hughes, Mollow quintuplets from coherently excited quantum dots, Opt. Lett. **38**, 1691 (2013).

[9] Y.-M. He, Y. He, Y.-J. Wei, D. Wu, M. Atatre, C. Schneider, S. Hfling, M. Kamp, C.-Y. Lu, and J.-W. Pan, On-demand semiconductor single-photon source with near-unity indistinguishability, Nat. Nanotechnol. **8**, 213 (2013).

[10] A. V. Kuhlmann, J. H. Prechtel, J. Houel, A. Ludwig, D. Reuter, A. D. Wieck, and R. J. Warburton, Transform-limited single photons from a single quantum dot, Nat. Commun. **6**, 8204 (2015).

[11] A. V. Kuhlmann, J. Houel, A. Ludwig, L. Greuter, D. Reuter, A. D. Wieck, M. Poggio, and R. J. Warburton, Charge noise and spin noise in a semiconductor quantum device, Nat. Phys. **9**, 570 (2013).

[12] M. J. Stanley, C. Matthiesen, J. Hansom, C. Le Gall, C. H. H. Schulte, E. Clarke, and M. Atature, Dynamics of a mesoscopic nuclear spin ensemble interacting with an optically driven electron spin, Phys. Rev. B **90**, 195305 (2014).

[13] D. Chen, G. R. Lander, K. S. Krowpman, G. S. Solomon, and E. B. Flagg, Characterization of the local charge environment of a single quantum dot via resonance fluorescence, Phys. Rev. B **93**, 115307 (2016).

[14] N. A. Vamivakas, Y. Zhao, C.-Y. Lu, and M. Atatre, Spin-resolved quantum-dot resonance fluorescence, Nat. Phys. **5**, 198 (2009).

[15] A. V. Kuhlmann, J. Houel, D. Brunner, A. Ludwig, D. Reuter, A. D. Wieck, and R. J. Warburton, A dark-field microscope for background-free detection of resonance fluorescence from single semiconductor quantum dots operating in a set-and-forget mode, Rev. Sci. Instrum. **84**, 073905 (2013).

[16] Y. He, Y.-M. He, J. Liu, Y.-J. Wei, H. Y. Ramirez, M. Atature, C. Schneider, M. Kamp, S. Hofling, C.-Y. Lu, and J.-W. Pan, Dynamically Controlled Resonance Fluorescence Spectra from a Doubly Dressed Single InGaAs Quantum Dot, Phys. Rev. Lett. **114**, 097402 (2015).

[17] D. Gammon, E. S. Snow, B. V. Shanabrook, D. S. Katzer, and D. Park, Fine Structure Splitting in the Optical Spectra of Single GaAs Quantum Dots, Phys. Rev. Lett. **76**, 3005 (1996).

[18] E. L. Ivchenko, Fine structure of excitonic levels in semiconductor nanostructures, Phys. Status Solidi A **164**, 487 (1997).

[19] M. Bayer, G. Ortner, O. Stern, A. Kuther, A. A. Gorbunov, A. Forchel, P. Hawrylak, S. Fafard, K. Hinzer, T. L. Reinecke, S. N. Walck, J. P. Reithmaier, F. Klopf, and F. Schafer, Fine structure of neutral and charged excitons in self-assembled In(Ga)As/(Al)GaAs quantum dots, Phys. Rev. B **65**, 195315 (2002).

[20] H. Tong and M. W. Wu, Theory of excitons in cubic III-V semiconductor GaAs, InAs and GaN quantum dots: Fine structure and spin relaxation, Phys. Rev. B **83**, 235323 (2011).

[21] F. Y. Wu, R. E. Grove, and S. Ezekiel, Investigation of the Spectrum of Resonance Fluorescence Induced by a Monochromatic Field, Phys. Rev. Lett. **35**, 1426 (1975).

[22] M. Metcalfe, G. S. Solomon, and J. Lawall, Heterodyne measurement of resonant elastic scattering from epitaxial quantum dots, Appl. Phys. Lett. **102**, 231114 (2013).

[23] N. H. Bonadeo, J. Erland, D. Gammon, D. Park, D. S. Katzer, and D. G. Steel, Coherent optical control of the quantum state of a single quantum dot, Science **282**, 1473 (1998).

[24] See Supplemental Material at http://link.aps.org/supplemental/10.1103/PhysRevLett.118.037401, which includes Refs. [25,26], for derivation of expressions for RPLE intensities and for details of data analysis methods.

[25] H. S. Nguyen, G. Sallen, M. Abbarchi, R. Ferreira, C. Voisin, P. Roussignol, G. Cassabois, and C. Diederichs, Photoneutralization and slow capture of carriers in quantum dots probed by resonant excitation spectroscopy, Phys. Rev. B **87**, 115305 (2013).

[26] S.-Y. Lu and R. A. Chipman, Interpretation of Mueller matrices based on polar decomposition, J. Opt. Soc. Am. A **13**, 1106 (1996).

[27] C. Cohen-Tannoudji and S. Reynaud, Dressed-atom description of resonance fluorescence and absorption spectra of a multi-level atom in an intense laser beam, J. Phys. B **10**, 345 (1977).

[28] R. Loudon, *The Quantum Theory of Light* (Oxford University Press, Oxford, 2000).

[29] G. Lindblad, On the generators of quantum dynamical semigroups, Commun. Math. Phys. **48**, 119 (1976).

[30] L. Allen and J. H. Eberly, *Optical Resonance and Two Level Atoms* (Wiley, New York, 1975).

[31] M. O. Scully and M. S. Zubairy, *Quantum Optics* (Cambridge University Press, Cambridge, 1997).

[32] T. Unold, K. Mueller, C. Lienau, T. Elsaesser, and A. D. Wieck, Optical Stark Effect in a Quantum Dot: Ultrafast Control of Single Exciton Polarizations, Phys. Rev. Lett. **92**, 157401 (2004).

[33] A. Muller, W. Fang, J. Lawall, and G. S. Solomon, Emission Spectrum of a Dressed Exciton-Biexciton Complex in a Semiconductor Quantum Dot, Phys. Rev. Lett. **101**, 027401 (2008).

[34] A. Muller, W. Fang, J. Lawall, and G. S. Solomon, Creating Polarization-Entangled Photon Pairs from a Semiconductor Quantum Dot Using the Optical Stark Effect, Phys. Rev. Lett. **103**, 217402 (2009).